Defect and coherent transient optical spectroscopy of rare earth doped crystals
by Guangming Wang

A thesis submitted in partial fulfillment of the requirements for the degree of Doctor of Philosophy in Physics
Montana State University

Abstract:
Spectral and structural properties of rare earth doped crystals have been investigated with white light absorption, fluorescence, fluorescence excitation, optically-detected nuclear-magnetic-resonance (ODNMR), photon echo and optical nutation.

Conventional spectroscopy was used to study Pr3+, Nd3+, Sm3+, Eu3+, Ho3+, Er3+ and Tm3"4" doped Y3Al5O12 crystals. Besides the intrinsic site spectroscopy, systematic studies on dopant ions in defect sites were carried out. There were generally 3-6 defect lines within ± 60 cm"1 of the intrinsic line. Quantitative optical absorption measurements showed that 4-7% of the dopants appeared in defect sites for the Eu3+, Ho3+, Er3+ and Tm3+ doped Y3Al5O12 crystals and 15-21% of the dopants appeared in defect sites for the Pr3+ and Nd3+ doped Y3Al5O12 crystals. These defects were attributed to the 1% of excess Y3+ substituting at Al3+ a sites (C3i symmetry) with a random distribution for Eu3+, Ho3+, Er3+ and Tm3"4" ions whose radii were close to Y3+ and a preferred distribution for Pr3+ and Nd3+ ions whose radii were much larger than Y3+.

Angle dependent ODNMR was used to determine the nuclear principal axis orientations of Pr3"4" ions in the intrinsic and defect sites of Pr3:Y3Al5O12. The intrinsic site has D2 symmetry which constrains the orientation of Pr3+ nuclear principal axes to specific directions. These directions were verified through ODNMR measurements. Using angle dependent ODNMR, one defect site was found to have C1 symmetry which is attributed to Y3+ substituting at Al3+ a sites.

Optical dephasing was studied for Tm3+:Y2Si2O7 as a function of temperature and laser excitation intensity via photon epho measurements. Temperature dependence of the optical dephasing was attributed to phonon coupling between the ground states 3H6(1) and 3H6(2) which were 6 cm"1 apart. Instantaneous spectral diffusion is another dephasing mechanism in this crystal. Using photon echoes, a homogeneous linewidth of 14 kHz was measured at 1.24 K for the 3H6(1) —> 3H4(1) transition. The relatively broad inhomogeneous linewidth of 100 GHz gave an inhomogeneous-to-homogeneous linewidth ratio of 7 x 106. This large ratio combined with a transition wavelength suitable for GaAlAs semiconductor lasers and the absence of hyperfine structure hole burning make this material an interesting candidate for time-domain signal processing and transient optically-addressed data storage.

Coherent transients were also studied for Tm3+:Y3Al5O12 via optical nutation measurements. Beats were observed due to the presence of several Rabi frequencies from the crystallographically-equivalent but orientationally-inequivalent crystal sites. Using symmetry considerations, we found for the first time that when the light electric field was along one of two special directions (111) and (001), the nutation had a single Rabi frequency. A general procedure for obtaining single Rabi frequency nutation (“single-dipole”) in arbitrary crystals is presented.

DEFECT AND COHERENT TRANSIENT OPTICAL SPECTROSCOPY OF RARE EARTH DOPED CRYSTALS

by

Guangming Wang

A thesis submitted in partial fulfillment
of the requirements for the degree

of

Doctor of Philosophy

in

Physics

MONTANA STATE UNIVERSITY
Bozeman, Montana

April, 1997

APPROVAL

of a thesis submitted by

Guangming Wang

This thesis has been read by each member of the thesis committee and has been found to be satisfactory regarding content, English usage, format, citations, bibliographic style, and consistency, and is ready for submission to the College of Graduate Studies.

18 April 1997
Date

Rufus L Cone
Chairman, Graduate Committee

Approved for the Major Department

4-18-97
Date

Head, Major Department

Approved for the College of Graduate Studies

5/8/97
Date

Graduate Dean

STATEMENT OF PERMISSION TO USE

In presenting this thesis in partial fulfillment of the requirements for a doctoral degree at Montana State University, I agree that the library shall make it available to borrowers under rules of the Library. I further agree that copying of this thesis is allowable only for scholarly purposes, consistent with "fair use" as prescribed in the U. S. Copyright Law. Requests for extensive copying or reproduction of this thesis should be referred to University Microfilms International, 300 North Zeeb Road, Ann Arbor, Michigan 48106, to whom I have granted "the exclusive right to reproduce and distribute my dissertation for sale in and from microform or electronic format, along with the right to reproduce and distribute my abstract in any format in whole or in part."

Signature 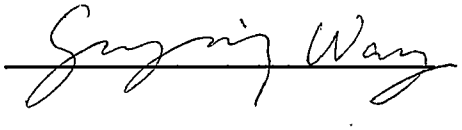

Date 4/18/1997

ACKNOWLEDGMENTS

The author is grateful to all those who gave their time, expertise and wise counsel to him during his graduate career. First and foremost, he wants to thank his advisor, Professor Rufus L. Cone; only with his countless advice and assistance, could this thesis become possible.

The author also wishes to acknowledge the technical assistance from Norman Williams and Erik Andersen, and for the useful discussion and assistance from his lab colleagues: Greg White, Charles Thiel, Todd Harris, Gregory Reinemer, Dr. Nicholas Strickland, Dr. Flurin Koenz, and Sebastien Ermeneux, special thanks to Dr. Yongchen Sun and Dr. Randy W. Equall for their relentless tutoring in running the experiments and analyzing the data.

The author is indebted to Dr. R. M. Macfarlane and Dr. M. J. M. Leask for their stimulating discussion and productive collaboration.

The author would like to thank Scientific Materials Corporation for providing high quality crystal samples.

Finally, the author would like to express his gratitude to his wife Bingbing Chen and his family for all of their love and encouragement over the years.

TABLE OF CONTENTS

TABLE OF CONTENTS — Continued

Page

TABLE OF CONTENTS — Continued

Page

LIST OF TABLES

Page

LIST OF TABLES — Continued

Page

LIST OF FIGURES

Page

LIST OF FIGURES — Continued

Page

LIST OF FIGURES — Continued

Page

LIST OF FIGURES — Continued

Page

LIST OF FIGURES — Continued

Page

LIST OF FIGURES — Continued

Page

LIST OF FIGURES — Continued

Page

ABSTRACT

Spectral and structural properties of rare earth doped crystals have been investigated with white light absorption, fluorescence, fluorescence excitation, optically-detected nuclear-magnetic-resonance (ODNMR), photon echo and optical nutation.

Conventional spectroscopy was used to study Pr^{3+}, Nd^{3+}, Sm^{3+}, Eu^{3+}, Ho^{3+}, Er^{3+} and Tm^{3+} doped $Y_3Al_5O_{12}$ crystals. Besides the intrinsic site spectroscopy, systematic studies on dopant ions in defect sites were carried out. There were generally 3-6 defect lines within $\pm$ 60 cm^{-1} of the intrinsic line. Quantitative optical absorption measurements showed that 4-7% of the dopants appeared in defect sites for the Eu^{3+}, Ho^{3+}, Er^{3+} and Tm^{3+} doped $Y_3Al_5O_{12}$ crystals and 15-21% of the dopants appeared in defect sites for the Pr^{3+} and Nd^{3+} doped $Y_3Al_5O_{12}$ crystals. These defects were attributed to the 1% of excess Y^{3+} substituting at Al^{3+} *a* sites (C_{3i} symmetry) with a random distribution for Eu^{3+}, Ho^{3+}, Er^{3+} and Tm^{3+} ions whose radii were close to Y^{3+} and a preferred distribution for Pr^{3+} and Nd^{3+} ions whose radii were much larger than Y^{3+}.

Angle dependent ODNMR was used to determine the nuclear principal axis orientations of Pr^{3+} ions in the intrinsic and defect sites of Pr^{3+}:$Y_3Al_5O_{12}$. The intrinsic site has D_2 symmetry which constrains the orientation of Pr^{3+} nuclear principal axes to specific directions. These directions were verified through ODNMR measurements. Using angle dependent ODNMR, one defect site was found to have C_1 symmetry which is attributed to Y^{3+} substituting at Al^{3+} *a* sites.

Optical dephasing was studied for Tm^{3+}:$Y_2Si_2O_7$ as a function of temperature and laser excitation intensity via photon echo measurements. Temperature dependence of the optical dephasing was attributed to phonon coupling between the ground states $^3H_6(1)$ and $^3H_6(2)$ which were 6 cm^{-1} apart. Instantaneous spectral diffusion is another dephasing mechanism in this crystal. Using photon echoes, a homogeneous linewidth of 14 kHz was measured at 1.24 K for the $^3H_6(1) \rightarrow {}^3H_4(1)$ transition. The relatively broad inhomogeneous linewidth of 100 GHz gave an inhomogeneous-to-homogeneous linewidth ratio of 7 x 10^6. This large ratio combined with a transition wavelength suitable for GaAlAs semiconductor lasers and the absence of hyperfine structure hole burning make this material an interesting candidate for time-domain signal processing and transient optically-addressed data storage.

Coherent transients were also studied for Tm^{3+}:$Y_3Al_5O_{12}$ via optical nutation measurements. Beats were observed due to the presence of several Rabi frequencies from the crystallographically-equivalent but orientationally-inequivalent crystal sites. Using symmetry considerations, we found for the first time that when the light electric field was along one of two special directions (111) and (001), the nutation had a single Rabi frequency. A general procedure for obtaining single Rabi frequency nutation ("single-dipole") in arbitrary crystals is presented.

CHAPTER 1

INTRODUCTION

Defect sites in crystals doped with trivalent rare earth ions have been studied extensively, but there are still many interesting and challenging questions waiting to be answered. This thesis studies the defects in rare earth ion doped $Y_3Al_5O_{12}$ crystals. In particular, the defects in Pr^{3+}, Nd^{3+}, Sm^{3+}, Eu^{3+}, Ho^{3+}, Er^{3+}, and Tm^{3+} doped $Y_3Al_5O_{12}$ crystals were systematically studied using conventional spectroscopic methods including white light absorption, fluorescence, and fluorescence excitation. Energy levels of the rare earth ion in defect sites were measured, and the intensities of the transitions were used to determine the defect site concentration. The local structure of one defect site in Pr^{3+} doped $Y_3Al_5O_{12}$ crystal was studied using nonlinear spectroscopic methods including optically detected nuclear magnetic resonance (ODNMR) and Raman heterodyne detection of NMR.

A better understanding of the defects is very helpful in improving laser efficiency, laser longevity and crystal growth techniques. Because the $Y_3Al_5O_{12}$ crystal has a relatively complex structure compared to other crystals, the techniques used in this thesis can also be applied to other crystals for defect or structural studies.

There are several excellent books on rare earth ion spectroscopy.[1-3] Readers are referred to these books for overviews. This chapter introduces several spectroscopic and structural topics: homogeneous broadening, inhomogeneous broadening, satellite lines in the spectra, crystal structure and selection rules for R^{3+} doped $Y_3Al_5O_{12}$, crystal growth and sample preparation, defects in R^{3+} doped $Y_3Al_5O_{12}$, and mechanisms for defect formation. These topics will provide the background for further discussion in the following chapters.

Homogeneous Broadening

Spectral lines of the rare earth ions in crystals are normally broadened by two major classes of mechanisms i.e. homogeneous broadening and inhomogeneous broadening. Homogeneous broadening arises from dynamic perturbations caused by lattice phonon coupling, nuclear or electron spin couplings and population decay. This broadening is experienced equally by all the ions but can be different for different energy levels. Within one J manifold, the splittings between different crystal field components are less than average phonon frequencies. When the upper crystal field components are excited, they nonradiatively decay to the lowest crystal field component through phonon coupling which increases their homogeneous linewidth. On the other hand, since the separation between J manifolds is often larger than the maximum phonon frequency at liquid helium temperatures, multiphonon emission is normally required to relax the lowest crystal field component. Therefore, the lowest component of a J-manifold has

smaller homogeneous broadening (kHz-MHz scale) than the upper crystal field components.

The lowest crystal field component is generally chosen for detailed spectroscopic studies for several reasons. Small broadening makes the satellite lines easily resolved around this lowest crystal field component. With little non-radiative decay, it is possible to detect fluorescence, apply optical pumping and use advanced nonlinear spectroscopic techniques. A long lifetime is also desirable for optical memory applications by allowing time for recording and retrieving optical data pulses.

Changes in temperature can dramatically change the homogeneous broadening by changing the phonon population. In order to reduce the homogeneous broadening, most of our experiments were done with the samples immersed in superfluid liquid helium pumped to a temperature of 1.4 K unless otherwise specified.

Inhomogeneous Broadening

No crystal is perfect; strains, impurities, and defects are common. For example, $Y_3Al_5O_{12}$ crystals are grown from the melt at high temperature. Compositions can change on a microscopic scale during growth introducing strains. When the crystals are cooled, static lattice strains are also introduced. Impurities may come from the raw oxide starting materials and from the melt crucible. Defects such as striae may appear when there are small temperature variations during the growth. Growth departing from the stoichiometric composition can also form local defects.

All of these perturbations will generate local environments with slightly different crystal fields. When the rare earth ions are doped into these various environments, the resulting distribution of transition frequencies for all the ions will have a typically Gaussian form; this is called inhomogeneous broadening. When the dopant concentration is high, the dopant ions themselves can also cause extra perturbations which will in turn inhomogeneously broaden the lines.

Inhomogeneous broadening usually completely dominates the linewidths of transitions of the lowest level in a given J manifold at temperatures below ~50 K. The inhomogeneous linewidth obscures other important spectroscopic parameters such as the homogeneous linewidth and hyperfine or superhyperfine splittings that are on the order of kHz - MHz. Advanced techniques are needed to extract these important parameters.

Satellite Lines in the Spectra

Impurities not only cause inhomogeneous broadening but may also give rise to additional lines in the absorption and emission spectra. This phenomenon was attributed to the formation of different impurity clusters, as a result of which a distribution of R^{3+} ions among different sites with different crystal fields occurred. This subject has been studied by many researchers. A recent paper was published by John Wright's group.[4] More detailed references will be provided for specific R^{3+}:$Y_3Al_5O_{12}$ crystals.

Using the conventional spectroscopic techniques described in Chapter 2, one can separate the spectra of R^{3+} ions with inequivalent crystallographic environments (activator centers) and consequently analyze the mechanism of cluster formation in

connection with the nature of the valence and size of the impurity ions and the specific crystal structure. This phenomenon is closely related to the laser performance of rare earth doped $Y_3Al_5O_{12}$ crystals. This thesis will classify and study $Y_3Al_5O_{12}$ defects with a variety of spectroscopic techniques.

Crystal Structure and Selection Rules for R^{3+} Doped $Y_3Al_5O_{12}$

The $Y_3Al_5O_{12}$ garnet crystal structure is shown in Figure 1. The ideal structure of the simple rare-earth garnets $A_3B_2C_3O_{12}$ is cubic O^{10}_h (Ia3d), and the unit cell contains eight molecules. In these garnets all the cations are trivalent; the *A* ions are rare-earth elements such as Pr^{3+}, Nd^{3+}, or group-III elements such as Y^{3+} located at dodecahedral *c* sites (with local D_2 symmetry), while the *B* and *C* ions are group-III elements such as Al^{3+} or Ga^{3+}. The *B* ions are placed in trigonally distorted octahedral *a* sites (C_{3i} symmetry), while the *C* ions occupy tetrahedral *d* sites (S_4 symmetry). Crystallographic data for $Y_3Al_5O_{12}$ is shown in Table 1.

The R^{3+} ions that substitute for Y^{3+} ions on the dodecahedral sites experience a crystal field of D_2 symmetry. There are six magnetically-inequivalent orientations of these sites in the crystal, as shown in Figure 2.[6] The local x, ý, and z axes of site 1 are oriented along the (110), $(1\bar{1}0)$ and (001) directions of the crystal with the z axis coinciding with the (001) axis by convention. The local axes of other sites can be obtained by applying the cubic symmetry operation.

Table 1. Crystallographic data for $Y_3Al_5O_{12}$. Cubic Ia3d, #230, Z = 8. X-ray data: a = 12.000 angstrom, x = -0.0306, y = 0.0512, z = 0.1500.[5]

Ion	Position	Symmetry	X	Y	Z
Y	24©	D_2	0	1/4	1/8
Al_1	16(*a*)	C_{3i}	0	0	0
Al_2	24(*d*)	S_4	3/8	0	1/4
O	96(*h*)	C_1	x	y	z

The D_2 point group contains four one-dimensional irreducible representations, Γ_1, Γ_2, Γ_3, and Γ_4. For R^{3+} ions with an even number of *f* electrons such as Pr^{3+} with a ($4f^2$) configuration, each $^{2S+1}L_J$ manifold is split into 2J+1 nondegenerate components, often called Stark levels. Table 2 gives the irreducible group representations for each value of J up to 6. From the multiplication tables given by Koster et al.,[7] the selection rules for electric-dipole and magnetic-dipole transitions can be determined and are summarized in Table 3. When the initial and final states have the same representation, the electric-dipole and magnetic-dipole transitions between them are forbidden.

Table 2. Full rotation compatibility table for the D_2 group[7]

J	Γ_1	Γ_2	Γ_3	Γ_4
0	1	0	0	0
1	0	1	1	1
2	2	1	1	1
3	1	2	2	2
4	3	2	2	2
5	2	3	3	3
6	4	3	3	3

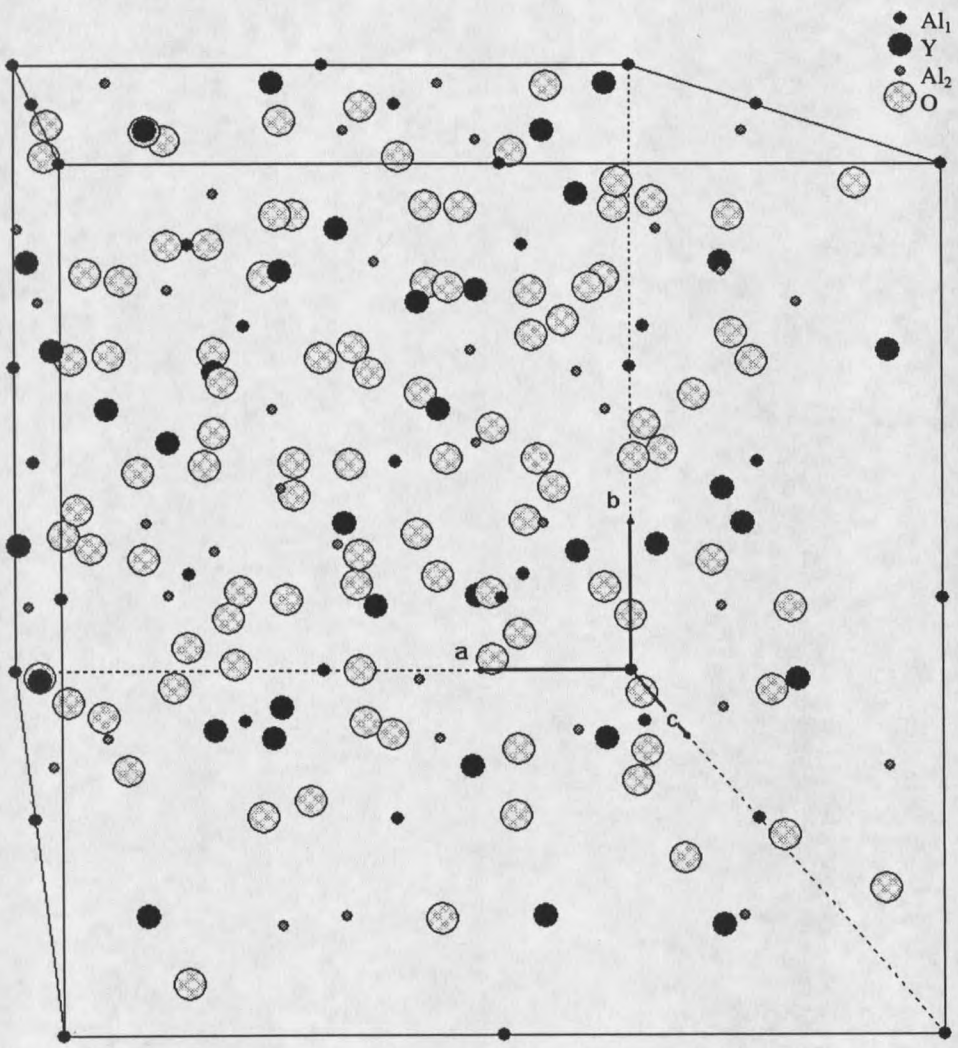

Figure 1. The very complex $Y_3Al_5O_{12}$ crystal structure. Al_1 represents the Al^{3+} ion in an *a* site and Al_2 represents the Al^{3+} ion in a *d* site. There are eight molecules and a total of 160 ions per unit cell.

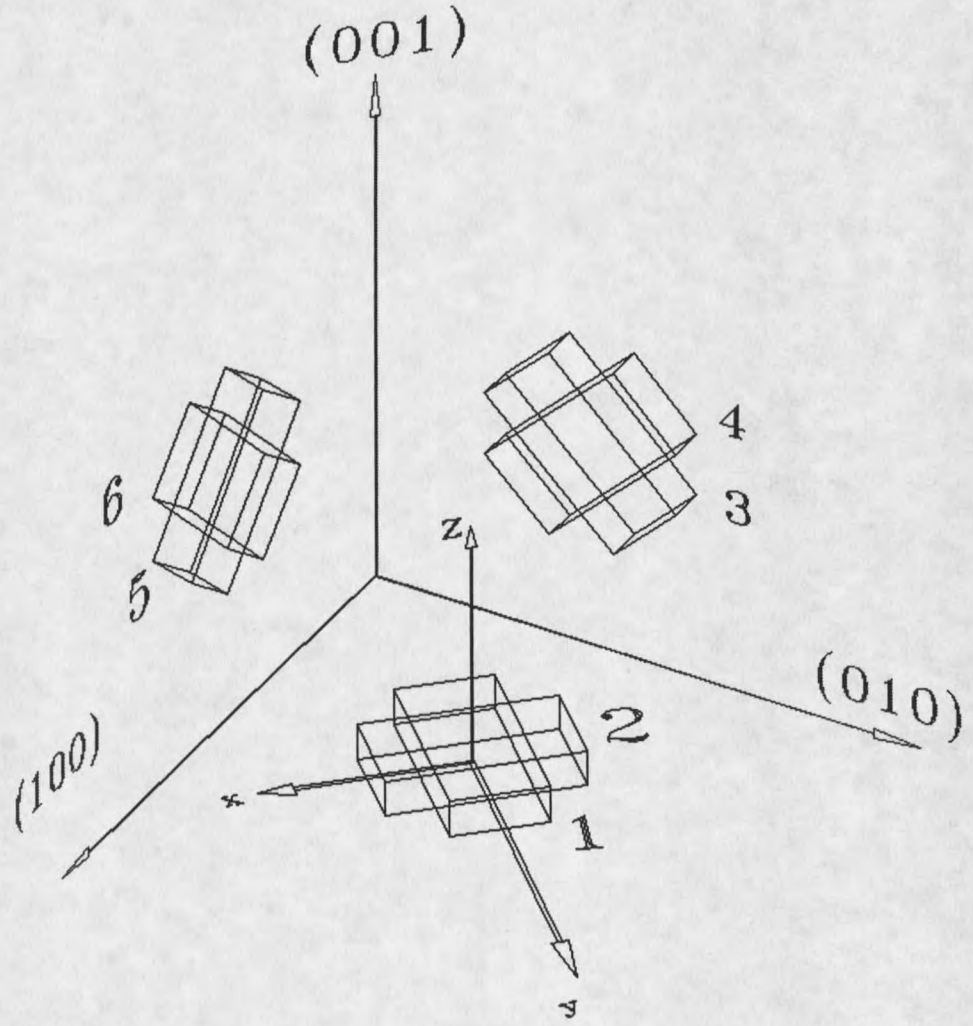

Figure 2. Orientation in the crystal lattice of the six orientationally-inequivalent sites of the Y^{3+} ion in the unit cell of yttrium aluminum garnet.[6] The rectangular boxes represent the local D_2 symmetries where each axis direction is different, and x, y and z are the local axes for site 1 of 6 sites.

Table 3. Electric-dipole and magnetic-dipole selection rules for D_2 symmetry. The Γ_i's are the representations of the initial & final states. E denotes electric-dipole; M, magnetic-dipole. The indices x, y, and z refer to the local site symmetry axes.

	Γ_1	Γ_2	Γ_3	Γ_4
Γ_1	-	E_y, M_y	E_z, M_z	E_x, M_x
Γ_2	E_y, M_y	-	E_x, M_x	E_z, M_z
Γ_3	E_z, M_z	E_x, M_x	-	E_y, M_y
Γ_4	E_x, M_x	E_z, M_z	E_y, M_y	-

For R^{3+} ions with an odd number of *f* electrons, such as Nd^{3+} ($4f^1$), each $^{2S+1}L_J$ manifold is split into (2J+1)/2 doubly-degenerate components. For an arbitrarily oriented crystal there are no restrictions by the selection rules for electric dipole transitions; hence, the crystal field levels of excited states can all be directly obtained from the absorption spectra.

Crystal Growth and Sample Preparation

Most of the samples studied in this thesis and their measured concentrations were provided by Scientific Materials Corporation in Bozeman, Montana. Growth of garnet materials has been carried out for more than 35 years and is technologically well advanced. Yttrium aluminum garnet is a congruently melting compound (m.p. 1970 °C). The dopant incorporation into the host crystal is governed by the following expression[8]

$$C_S = kC_L \tag{1.1}$$

where C_S is the dopant concentration in the solid, C_L is the starting melt composition, and k is the distribution of the dopant between the solid and liquid phases. The value of k is

ordinarily less than unity and depends markedly upon the dopant radius and growth condition.[8]

Pure R_2O_3, Y_2O_3, and Al_2O_3 powder is mixed and melted in a crucible to growth R^{3+}:$Y_3Al_5O_{12}$ crystal. The maximum R^{3+} concentration is limited by the ionic radius mismatch between relatively large rare earth ions and smaller aluminum ions. In the extreme end, the rare earth garnet $R_3Al_5O_{12}$ grown from three part R_2O_3 and five part Al_2O_3 mixture is found only for the R^{3+} ions between Gd^{3+} and Lu^{3+}. Ions larger than Gd^{3+} do not form garnets in the simple two oxide system. However, a garnet crystal with low concentration of ions from Ce^{3+} to Sm^{3+} can be formed from the molten phase.

Single crystals used in this study were grown parallel to the (111) direction by the Czochralski technique from yttrium aluminum garnet melts doped with R^{3+} oxide. Normally rods about 5mm in diameter were cut from the boules parallel to the (111) direction. Two end faces were polished to optical quality. Most white light absorption experiments were done along (111). The sides of some rods were polished for fluorescence experiments. Most crystals studied in this thesis have low dopant concentration for high resolution spectroscopy, hence, they are colorless.

Defects in R^{3+} Doped $Y_3Al_5O_{12}$ and Mechanisms for Defect Formation

Doping of garnet crystals with R^{3+} ions is expected to lead to the appearance of a very limited variety of structural centers, according to the site preference of the dopant. Conventionally, one assumes that only the transitions belonging to a single structural center (D_2 site for the R^{3+} doped garnet) exist, but this is not the case in practice. A much

more complex behavior is observed in optical spectra. The multisite structure of R^{3+} ions in garnet crystals is not a completely elucidated problem, and is a major focus of this thesis. The analysis of defect structures requires further attention, due to the structural information that can be obtained, the impact on laser design, and information on the R^{3+} - R^{3+} interaction mechanisms. One objective of this thesis is to develop a better understanding of structural defects, using both conventional spectroscopy and nonlinear spectroscopy.

The ideal garnet has the compound formula $A_3B_2C_3O_{12}$, where *A*, *B*, *C* ions occupy the dodechedral D_2 *c* site, the octahedral C_{3i} *a* site, and the tetrahedral S_4 *d* site, respectively. Lattice parameter measurements using X-ray powder diffraction on rare-earth gallium garnets have shown that the compositions of garnet crystals grown from the melt are different from the compositions of stoichiometric ceramic samples.[9,10] This difference is attributed to an excess (up to several percent as a function of composition) of *A* ions occupying the octahedral sites; the composition can be written as $A_3(B_{1-x}A_x)_2C_3O_{12}$. The value x may vary depending on the synthesis temperature, the composition of the melt, and the type of RE ions. For $Y_3Al_5O_{12}$ crystals grown from the melt at 1970 °C, the estimated formula is $Y_3(Al_{0.985}Y_{0.015})_2Al_3O_{12}$.[9]

Several types of optical spectra for R^{3+}:$A_3B_2C_3O_{12}$ have been investigated by a number of groups:[11-14]

(1) the main spectrum, corresponding to R^{3+} in unperturbed dodecahedral *c* sites,

(2) satellite lines, whose relative intensity does not depend on R^{3+} content, assigned to R^{3+} in *c* sites perturbed by the presence of *A* ions in anomalous *a* sites,

(3) satellite lines, whose relative intensity does depend on dopant concentration, assigned to the near-neighbor pairs of R^{3+} ions in *c* sites,

(4) weak lines assigned to R^{3+} in octahedral *a* sites,

(5) lines arising from the perturbation by anionic impurities such as OH^-.

Spectra of type (1) are usually studied first. Energy levels can be readily determined using the selection rules for D_2 symmetry given in Table 3. This provides the starting point for studying the satellite lines. Spectra of types (2), (3), and (5) originate from R^{3+} ions in perturbed dodecahedral *c* sites. Normally for each type, there are several weak lines surrounding the main line of type (1); these three types have different properties such as fluorescence lifetime and energy transfer rate, and their properties are closely related to the local environment. Spectra of type (4) originate from R^{3+} ions in the C_{3i} site and have selection rules quite different from those in Table 3. Different types of the defect spectra mentioned above may dominate depending on the dopant concentration, dopant radius, and host crystals. Spectrum types (1), (2), and (4) were observed and will be explained in this thesis. More work needs to be done to correlate the spectrum type (5) to OH^- impurity by comparing samples with different OH^- concentrations.

In order to have a quantitative study of the defect lines, we need to consider the distributions of R^{3+} ions and of the defects in the crystal. Substitution of trivalent *A* ions by R^{3+} activators does not require charge compensation, and therefore there is no reason

for an electrostatic-interaction correlation in their distribution in the lattice. Since at low concentration the difference in the ionic radii between an R^{3+} ion and the host cation A normally does not lead to size correlation, the most likely model for R^{3+} distribution in garnets is random uniform occupancy of the available sites. Similar arguments are valid for other structural defects such as anomalous A ions in octahedral sites.[15]

For a random uniform distribution of activators, the probability of occurrence of ensembles formed by a given activator ion with n neighbor activators in a sphere with m sites is given by[16]

$$C_{nm} = \frac{m!}{n!(m-n)!} C^{n+1}(1-C)^{m-n}, \tag{1.2}$$

where C is the concentration of activators. For low C values, the most probable ensembles are pairs, i.e., $n = 1$. From Eq. (1.2), the pair concentration is $C_{1m} = mC^2(1-C)^{m-1}$. For low dopant such as $C = 0.1\%$ the pair concentration is negligible (~ 1ppm).

The probability of occurrence of ensembles formed by a given activator ion with n' neighbor defects in a sphere with m' sites is given by[16]

$$C_{n'm'} = \frac{m'!}{n'!(m'-n')!} C(C')^{n'}(1-C')^{m'-n'}, \tag{1.3}$$

where C' is the concentration of defects. The most probable ensembles are with one defect neighbor, i.e., n'=1, whose concentration is $C_{1m'} = m'CC'(1-C')^{m'-1}$. When C' is a few percent, these clusters make a significant contribution to the defect lines.

The number of sites in the neighboring spheres around different sites and the radii of these spheres for $Y_3Al_5O_{12}$ are given in Table 4.